# 3d–4f Magnetic Interaction with Density Functional Theory Plus U Approach: Local Coulomb Correlation and Exchange Pathways

**3 AUTHORS**, INCLUDING:

Yachao Zhang
Guizhou Education University

**4** PUBLICATIONS **15** CITATIONS

SEE PROFILE

Hong Jiang
Peking University

**53** PUBLICATIONS **797** CITATIONS

SEE PROFILE

# 3d−4f Magnetic Interaction with Density Functional Theory Plus $U$ Approach: Local Coulomb Correlation and Exchange Pathways

Yachao Zhang, Yang Yang,[†] and Hong Jiang*

Beijing National Laboratory of Molecular Sciences, State Key Laboratory of Rare Earth Materials Chemistry and Applications, College of Chemistry and Molecular Engineering, Peking University, Beijing 100871, China

**S** *Supporting Information*

**ABSTRACT:** The 3d−4f exchange interaction plays an important role in many lanthanide based molecular magnetic materials such as single-molecule magnets and magnetic refrigerants. In this work, we study the 3d−4f magnetic exchange interactions in a series of Cu(II)−Gd(III) $(3d^9−4f^7)$ dinuclear complexes based on the numerical atomic basis-norm-conserving pseudopotential method and density functional theory plus the Hubbard $U$ correction approach (DFT+$U$). We obtain improved description of the 4f electrons by including the semicore 5s5p states in the valence part of the Gd-pseudopotential. The Hubbard $U$ correction is employed to treat the strongly correlated Cu-3d and Gd-4f electrons, which significantly improve the agreement of the predicted exchange constants, $J$, with experiment, indicating the importance of accurate description of the local Coulomb correlation. The high efficiency of the DFT+$U$ approach enables us to perform calculations with molecular crystals, which in general improve the agreement between theory and experiment, achieving a mean absolute error smaller than 2 cm$^{-1}$. In addition, through analyzing the physical effects of $U$, we identify two magnetic exchange pathways. One is ferromagnetic and involves an interaction between the Cu-3d, O-2p (bridge ligand), and the majority-spin Gd-5d orbitals. The other one is antiferromagnetic and involves Cu-3d, O-2p, and the empty minority-spin Gd-4f orbitals, which is suppressed by the planar Cu−O−O−Gd structure. This study demonstrates the accuracy of the DFT+$U$ method for evaluating the 3d−4f exchange interactions, provides a better understanding of the exchange mechanism in the Cu(II)−Gd(III) complexes, and paves the way for exploiting the magnetic properties of the 3d−4f compounds containing lanthanides other than Gd.
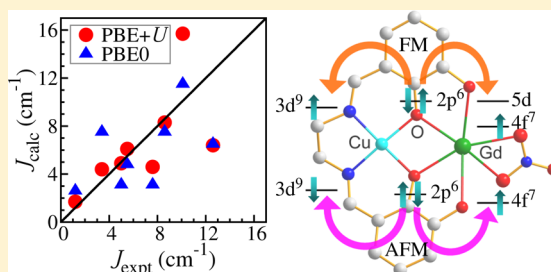
## 1. INTRODUCTION

The 3d−4f exchange interactions in complexes containing transition-metal (TM) ions and lanthanides (Ln) have attracted a lot of interests due to their importance in building molecular magnetic materials.[1,2] First, 3d−4f molecular clusters are promising candidates for single-molecule magnets (SMMs).[3−5] This is because the partially filled Ln-4f shells exhibit large spin magnetic moments $S$ and significant spin−orbit coupling (SOC) effects that are crucial for generating the desired high magnetic anisotropy barriers of SMMs.[6] Second, isotropic 3d−4f interactions (e.g., in TM−Gd(III) systems) are favorable in producing working materials for magnetic refrigerants,[7,8] which function on the basis of field-dependent magnetocaloric effect (MCE). The MCE is primarily induced by the entropy change of the magnetic system upon switching on external magnetic field. Because of the strong localization nature of the 4f orbitals, the 3d−4f exchange interactions (typically several cm$^{-1}$)[9] are much weaker than the 3d−3d exchange couplings (hundreds of cm$^{-1}$).[10,11] The weak exchange interactions give rise to multiple low-lying excited spin states, which increase the magnetic degrees of freedom or the magnetic entropies of the system. These effects along with the large spin $S$ result in more pronounced MCE than that of the TM complexes.[12]

From the theoretical point of view, predicting the magnetic properties of these materials requires the accurate determination of the 3d−4f interactions.[13] The latter relies on accurate description of the localization behaviors[14] of the 3d and 4f magnetic orbitals. However, the Coulomb correlations among electrons in the 3d and 4f shells are poorly described[15,16] within the standard local density or generalized gradient approximations (LDA/GGA) of density functional theory (DFT) due to the self-interaction error (SIE).[17,18] The predicted d/f electron densities under LDA/GGA are delocalized unphysically so that the magnetic interactions are overestimated.[19] Although some correlated quantum chemistry methods (e.g., CASSCF/CASPT2[20]) and hybrid functionals[19] considerably improve the description, these approaches are practically not applicable to extended systems with hundreds of atoms per cell. This problem can be remedied by introducing some corrections to LDA/GGA such as the self-interaction correction (SIC)[17,21,22] or the Hubbard-$U$ correction (DFT+$U$).[23,24] It has been shown that the (DFT+$U$) method can reliably

reproduce the experimental magnetic interactions for the 3d–3d systems.[25,26]

Another obstacle in studying 3d–4f interactions arises from the relativistic effects of the 4f electrons, including SOC and scalar-relativistic (SR) effects (mass-velocity and Darwin terms).[27] The ground states of Ln ions (except Gd(III) and Eu(II)) have large unquenched first-order orbital momenta $\mathbf{L}$[28] due to the poor participation of the 4f orbitals in the chemical bonds. Thus, the SOC term should be added into the isotropic Heisenberg–Dirac–Van Vleck (HDVV) spin Hamiltonian,[29] in which case the extraction and analysis of the exchange interactions becomes a difficult task.[9] For this reason, current theoretical studies of the 3d–4f exchange interactions mainly focus on Cu(II)–Gd(III) compounds.[19,20,30] There is no first-order SOC for Gd(III) (with $\mathbf{L} = 0$), and the coupling between the ground state and the first excited state is negligible.[31] Thus, the Cu(II)–Gd(III) systems are almost perfectly isotropic. In addition, the 3d–4f interactions in Cu(II)–Gd(III) compounds are ferromagnetic, almost irrespective of the nature of the ligands.[9] The underlying mechanism[20] implies general magneto-structural correlations in the Ln–TM complexes.

Besides the SOC term, it is crucial to incorporate the SR corrections for reproducing the 3d–4f exchange interactions accurately.[19,30] Approaches for SR corrections include (i) all-electron (AE) calculations with approximate relativistic Hamiltonians (e.g., zeroth-order regular approximation (ZORA)[32] and Douglas–Kroll–Hess (DKH)[33,34]), (ii) calculations using relativistic effective core potentials (ECP) such as Los Alamos (LANL)[35] and Stuttgart–Dresden (SD)[36] ECPs, and (iii) methods based on first-principles pseudopotentials (PP)[37,38] incorporating the SR effects. The PP method can achieve a reasonable accuracy with much lower computational efforts compared to the AE methods and therefore has become the most widely used approach in materials simulations.[39]

For the Ln-PP, 4f states should be treated explicitly in the valence part to acquire sufficiently good transferability.[40,41] Despite their poor participation in the Ln-ligand bonding, the unpaired 4f electrons play special roles in the spin polarization of the surrounding chemical environment, which has been shown to be vital for the 3d–4f interactions.[13,30] Next, because the compact 4f orbitals are shielded by the closed-shell 5s5p states (Figure 1), the latter should also be put into the valence
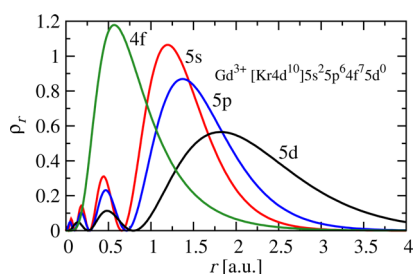


**Figure 1.** Radial charge density $\rho_r = r^2 R_l^2$ of the 5s, 5p, 4f, and 5d orbitals of the Gd(III) ion.

region.[42–45] These considerations make the Ln-PP very hard, requiring large basis sets and/or a fine numerical grid, particularly for the norm-conserving pseudopotentials (NCPP).[46]

In this work, we study the 3d–4f exchange interactions in Cu(II)–Gd(III) model compounds with the DFT+$U$ approach based on real-space numerical atomic basis-NCPP method as

implemented in the SIESTA code.[47] First, we show that it is necessary to treat the semicore 5s5p shells in the valence part of Gd-pseudopotential for an accurate description of the 4f orbitals. Second, we assess the accuracy of the DFT+$U$ approach for evaluating the exchange coupling constant $J$ using model complexes in both isolated molecular (molecular model) and periodic crystalline forms (crystal model). The accuracy of the DFT+$U$ approach is comparable with those of hybrid functionals in terms of the results obtained from molecular model. The calculated $J$s from the crystal model are better in agreement with experiment than those from the molecular model calculations, indicating the importance of the crystal packing effects. Third, we explore the physical effects of the local Coulomb correlation introduced by the Hubbard $U$ correction. We monitor the evolution of the charge/spin distribution and the underlying electronic structures upon switching on $U$ on specified atomic sites. It shows that the spin delocalization effect of the 3d orbitals is suppressed, while the spin polarization effect induced by the 4f orbitals is enhanced. The variation of the corresponding $J$ values indicates a ferromagnetic and an antiferromagnetic exchange pathways. The former involves Cu-3d, O-2p, and the majority-spin Gd-5d orbitals, while the latter involves Cu-3d, O-2p, and the empty minority-spin Gd-4f orbitals and tends to be weakened by the planar Cu–O–O–Gd structure.

This article is organized as follows. Section 2 provides details for the generation of Gd-PPs, methods and model systems for evaluating $J$, and simulation packages and the related parameters used in the calculations. In section 3.1, transferability and convergence tests of the generated Gd-PPs are provided. The predicted results of $J$ are shown in section 3.2. Section 3.3 is dedicated to the analysis of the physical effects of the Hubbard $U$, which sheds light on the 3d–4f exchange mechanism. Section 4 summarizes the main findings of this work and closes the article with some general remarks.

## 2. COMPUTATIONAL DETAILS

The NCPPs of Gd are generated following the Troullier–Martins procedure[48] with the ionic reference configurations [Xe]$4f^7 5d^0 6s^0 6p^0$ and [Kr$4d^{10}$]$5s^2 5p^6 4f^7 5d^0$, where the 5s5p shells are included in either the core (NCPP1) or the valence (NCPP2) part. For NCPP1, the cutoff radii $r_c$ of the valence 4f, 5d, 6s, and 6p orbitals are 1.50, 2.18, 2.60, and 2.80 au, respectively. For NCPP2, the $r_c$s of the 5s, 5p, 4f, and 5d orbitals are chosen to be 2.00, 2.00, 1.50, and 2.18 au, respectively. The inaccuracy introduced in the unscreening procedure due to the nonlinear dependence of exchange-correlation potentials on electron density is remedied by the nonlinear core correction (NLCC),[49] where the cutoff radius for the pseudocore $r_{pc}$ is set to 0.70 au. Relativistic effects including SOC are incorporated by solving the Dirac equation, while SOC is not included in practical calculations of molecules and solids. The procedures above are carried out using the pseudopotential generator in the SIESTA code.[47] To check the accuracy of the generated PPs, we perform calculations with the projector augmented wave (PAW)[50,51] method as implemented in Vienna ab initio Simulation Package (VASP).[52–54] Details about the test calculations of the Gd-PPs can be found in the Supporting Information. All the other PPs used in this work are taken from the pseudopotential database[55] supplied by the SIESTA team.

The exchange interaction is described by the isotropic Heisenberg Hamiltonian

$$\hat{H} = -J\hat{S}_A \cdot \hat{S}_B \tag{1}$$

where $\hat{S}_A$ and $\hat{S}_B$ denote spin operators corresponding to the two interacting magnetic centers A and B. The coupling constant $J$ is evaluated employing the spin-projected broken symmetry model[64,65]

$$J = \frac{E_{BS} - E_{HS}}{2S_A S_B} \tag{2}$$

Here $S_A$ and $S_B$ are spin quantum numbers of the two magnetic centers; HS and BS denote high spin state and broken symmetry state with parallel and antiparallel alignment of the interacting magnetic moments in each molecular unit, respectively. Both HS and BS states are obtained by spin-polarized calculations initialized by the desired magnetic configurations and fixed spin moments. It should be emphasized that the above procedure for extracting $J$ is only applicable to isotropic exchange couplings as in the Cu(II)−Gd(III) compounds. For other lanthanides with nonzero **L**, the spin Hamiltonian should be modified to include the SOC term, and thus, the extraction of $J$ becomes much more difficult.[9] Geometries of the model compounds (Table 1) both in

**Table 1. Cu···Gd Distances (in Å), Cu−O−O−Gd Dihedral Angles (in deg), and Experimental J Values (in cm$^{-1}$) of the Model Compounds**

| ref code | Cu···Gd | Cu−O−O−Gd | $J_{expt}$ | ref |
|---|---|---|---|---|
| AWUQUE | 3.443 | 161.1 | 5.0 | 56 |
| BERPAQ | 3.454 | 160.8 | 5.5 | 57 |
| FAKLOT | 3.454 | 168.9 | 8.6 | 58 |
| GANFIL | 3.498 | 170.7 | 7.6 | 59 |
| KEQRED | 3.512 | 178.3 | 10.1 | 60 |
| LAMBUX | 3.401 | 177.9 | 12.6 | 61 |
| OFELAM | 3.288 | 146.9 | 1.2 | 62 |
| XAYTIB | 3.346 | 159.5 | 3.4 | 63 |

molecular (Figure 2, *xyz* files are provided in the Supporting Information) and crystalline forms are taken directly from X-ray crystal structures[56−63] without relaxation. Both intra- and intermolecular magnetic dipolar interactions are ignored in this work. The results of $J$ are normalized by the number of the molecular units in the simulation cells.

Calculations using the Perdew−Burke−Ernzerhof (PBE)[66] exchange-correlation functional and the PBE+$U$ approach are carried out in the local version of the SIESTA code,[67] which employs real-space numerical pseudoatomic orbital (PAO)[68] basis and NCPP. We use triple-$\zeta$ plus the polarization (TZP) basis sets to describe the magnetic centers Cu and Gd, and use DZP for the remaining atoms. The parameter "energy shift"[69] that defines the confinement of the PAOs[70] is set to 50 meV. The fineness of the real-space grid, onto which electron densities and wave functions are projected to calculate the Kohn−Sham potentials and matrix elements, is controlled by the parameter *meshcutoff*,[71] which is set to 200 Ry. For self-consistent field (SCF) convergence, we employ a tolerance value of $10^{-6}$ for the density matrix and $10^{-4}$ (eV) for the total energy.

All SIESTA calculations employ periodic boundary conditions (PBC). In the case of an isolated molecule, an orthorhombic supercell is built with a lattice constant slightly larger (by 10%) than the minimum size that can accommodate

the molecule. Considering the large sizes of the simulation cells, only the $\Gamma$ point is used for the Brillouin zone sampling.

The PBE+$U$ calculations rely on implementations according to the simplified rotationally invariant formulations,[72] where only $(U - J)$[73,74] (difference between on-site Coulomb repulsion and exchange) is effective and will be denoted by $U$ below. The DFT+$U$ total energy functional depends explicitly on both the electron density $\rho$ and the local density matrix **n** for correlated orbitals

$$E_{DFT+U}[\rho] = E_{LDA/GGA}[\rho] + \frac{U}{2}\sum_{I,\sigma} \text{Tr}[\mathbf{n}^{I\sigma}(1 - \mathbf{n}^{I\sigma})] \tag{3}$$

where $\mathbf{n}^{I\sigma}$ refers to the occupation matrix of the localized orbitals (with spin index $\sigma$) in the correlated subspace (defined by localized projectors[75]) on atomic site $I$. The introduced Hubbard-like term (second term on the right side of eq 3) imposes an energy penalty for fractional occupations[76] and thus tends to get rid of the self-interaction error of LDA/GGA in describing the localized electrons. Here $U$ is a physical parameter that characterizes the on-site Coulomb repulsions among localized d/f electrons. It can be determined experimentally by (inverse) photoelectron spectra (PES/IPS)[77] or in a first-principles way by constrained density functional theory (cDFT) calculations[76,78−81] or constrained random phase approximation (cRPA).[82,83] According to previous cDFT calculations,[79,84−86] we choose the value of $U$ to be 6.0 eV for both the correlated Cu-3d and Gd-4f orbitals.

Hybrid functionals calculations, including Becke's three parameter exchange functional[87,88] combined with Lee−Yang−Parr correlation functional[89] (B3LYP) and PBE-based parameter-free hybrid functional PBE0,[90,91] are performed with the quantum chemistry code ORCA.[92] We employ all-electron scalar-relativistic TZP-ZORA[93,94] plus the Alrichs (d,p) polarization functions as basis sets and use Lebedev grid with 302 points (Grid4 in the ORCA code convention) for numerical integrations in the SCF iterations. We set a tight SCF convergence threshold, for which the total energy convergence criterion is $10^{-8}$ Hartree. The resolution of the identity (RI) approximation[95] is not switched on in our calculations.

## 3. RESULTS AND DISCUSSION

**3.1. Pseudopotentials of Gd.** To test the transferability of the generated NCPPs of Gd, we perform geometry optimization of the hexagonal $Gd_2O_3$ (Figure 3a) and a Cu(II)−Gd(III) dinuclear complex $[LCuGd(H_2O)_4]^{3+}$ (ref code KEQRED) where L is a Schiff base ligand (Figure 3b), employing NCPP1 and NCPP2 with the PBE functional. We compare the optimized structures to those obtained by the PAW method that is capable of reproducing the all-electron results.[51] Here we focus on the lattice constants and volume of the hexagonal $Gd_2O_3$ unit cell and the Gd−O bond lengths in the $[LCuGd(H_2O)_4]^{3+}$ molecule (Figure 3). The maximum relative absolute errors of NCPP1 (NCPP2) results with respect to the PAW results are shown to be 1.6% (1.0%), 4.7% (1.3%), and 2.4% (1.6%) for lattice constants, cell volume, and Gd−O bond lengths, respectively (Table 2). This comparison shows that NCPP2 agrees better with the PAW method than NCPP1.

We further compare the density of states (DOS) of $Gd_2O_3$ provided by calculations with NCPP1 and NCPP2 (Figure 4) to examine their performance in describing electronic
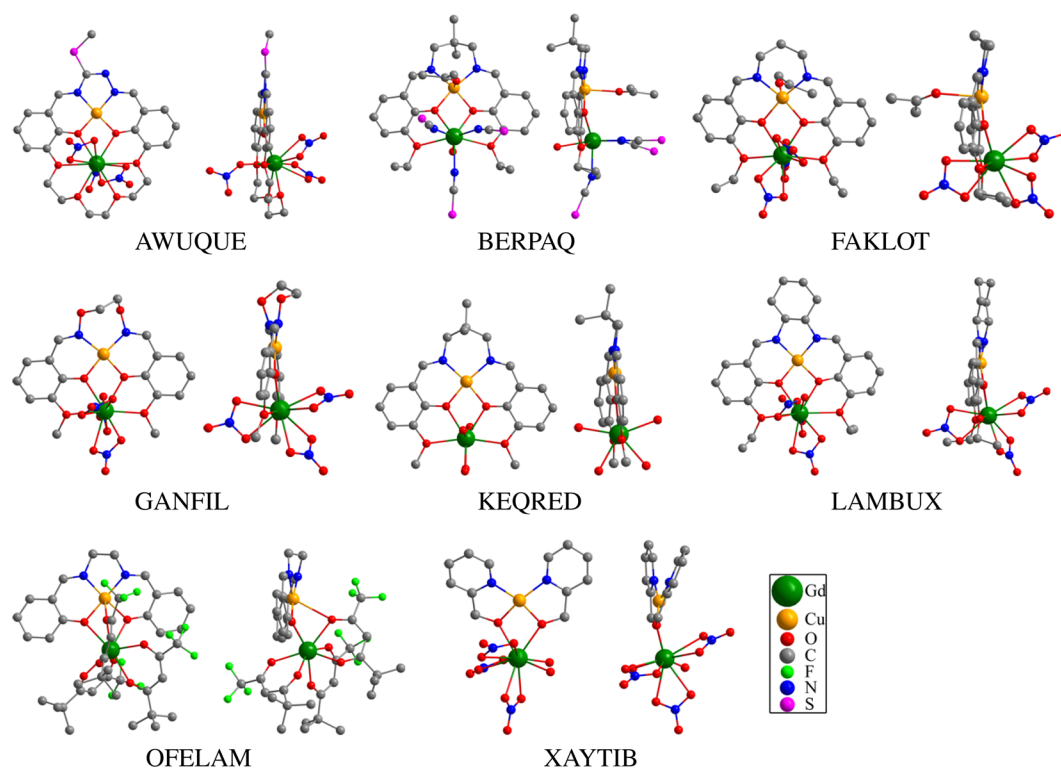
**Figure 2.** Molecular structures of the model compounds. For each molecule, we display front (left) and side (right) views. Hydrogen atoms are omitted for clarity.
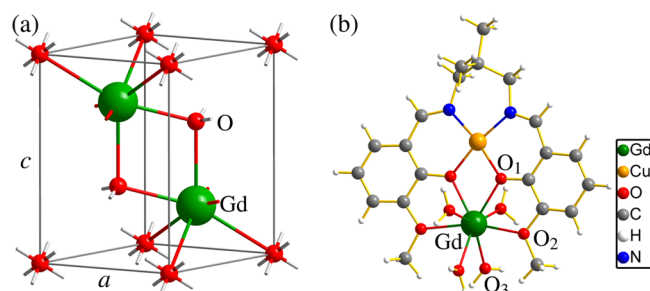


**Figure 3.** (a) Hexagonal unit cell of $Gd_2O_3$. (b) Molecular structure of $[LCuGd(H_2O)_4]^{3+}$ (KEQRED).



**Figure 4.** Calculated total density of states (DOS) of $Gd_2O_3$ using NCPP1 (dash line), NCPP2 (solid line), and the PAW method (filled curve). The valence band maximum (VBM) is set to 0 eV.

**Table 2. Optimized Lattice Constants ($a$, $c$ in Å) and Cell Volume ($V$ in Å$^3$) of the $Gd_2O_3$ Hexagonal Unit Cell (Figure 3a) and Gd−O Bond Lengths (Å) in $[LCuGd(H_2O)_4]^{3+}$ (Figure 3b) Using the Two Generated NCPPs and the PAW Method**

|  | NCPP1 | NCPP2 |  |
| --- | --- | --- | --- |
|  | $[Xe]4f^7$ | $[Kr4d^{10}]5s^25p^64f^7$ | PAW |
| $Gd_2O_3$ |  |  |  |
| $a$ [Å] | 3.68 | 3.75 | 3.74 |
| $c$ [Å] | 5.87 | 5.88 | 5.94 |
| $V$ [Å$^3$] | 68.5 | 71.0 | 71.9 |
| $[LCuGd(H_2O)_4]^{3+}$ |  |  |  |
| Gd−O$_1$ [Å] | 2.31 | 2.29 | 2.29 |
| Gd−O$_2$ [Å] | 2.46 | 2.46 | 2.48 |
| Gd−O$_3$ [Å] | 2.47 | 2.49 | 2.53 |

structures. Using the PAW result as a benchmark, we find that the occupied main peak (4f states) given by NCPP1 is slightly broadened, indicating that NCPP1 overestimates the Gd−O
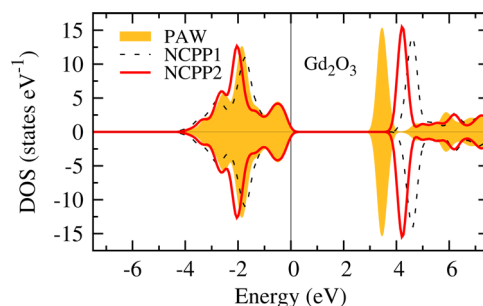
hybridizations. That is probably why NCPP1 predicts considerably smaller lattice constants and cell volume of $Gd_2O_3$. In contrast, the DOS given by NCPP2 is much better in agreement with the PAW result. Thus, NCPP2 will be used in the following calculations.

Next, we test the hardness of the generated PPs. Treating the 5s5p states in the valence region considerably increases the hardness of NCPP2, which requires larger basis sets than NCPP1 for a good representation of the valence states. Fortunately, the required size of the atomic-like basis[68] employed in SIESTA is not as sensitive as the plane waves basis sets. Converged $J$ values can be obtained using the standard TZP basis sets.[13] However, it still requires a rather fine real-space grid, the density of which is controlled by *meshcutoff* in SIESTA. Convergence test with respect to this parameter is performed by calculating the 3d−4f exchange coupling constant $J$ of the model complex (shown in Figure 3b) using the PBE functional. It shows that well converged results (with variation within 0.5 cm$^{-1}$) have been obtained at 100 Ry for NCPP1 and

125 Ry for NCPP2 (Table 3). This parameter in our following calculations is set to 200 Ry, which should be large enough for obtaining converged results.

**Table 3. Calculated $J$ (cm$^{-1}$) in the KEQRED Molecule (Figure 3b) Employing the Generated NCPPs with Respect to Parameter *meshcutoff* (Ry) That Controls the Fineness of the Numerical Grid**

|  | NCPP1 | NCPP2 |
| --- | --- | --- |
| *meshcutoff* | [Xe]4f$^7$ | [Kr4d$^{10}$]5s$^2$5p$^6$4f$^7$ |
| 75 | 23.3 | not conv$^a$ |
| 100 | 21.4 | 28.3 |
| 125 | 21.7 | 18.6 |
| 150 | 21.7 | 18.6 |
| 200 | 21.4 | 18.8 |
| 250 | 21.4 | 18.3 |
| 300 | 21.3 | 18.5 |

$^a$Not converged to desired magnetic configurations required by the BS approach for extracting $J$.

**3.2. Evaluating $J$.** In this section, we assess the accuracy of PBE+$U$ for evaluating the 3d−4f magnetic interactions based on the SIESTA code. Eight Cu(II)−Gd(III) model complexes are chosen with the experimental $J$ values (Table 1) covering a relatively wide range (1−13 cm$^{-1}$).[30] First, we perform calculations with the molecular model. PBE, PBE+$U$ ($U$ is turned on for 3d/4f at specified atomic sites: Cu-3d only, PBE+$U_{3d}$; Gd-4f only, PBE+$U_{4f}$; both Cu-3d and Gd-4f, PBE+$U_{3d4f}$), and hybrid functionals (B3LYP and PBE0) are employed in these calculations (Table 4). It shows that neither PBE nor PBE+$U_{4f}$ can predict right signs of $J$ for all the model compounds, whereas PBE+$U_{3d}$ and PBE+$U_{3d4f}$ give much improved results that are well consistent with those of the hybrid functionals.

In particular, PBE+$U$ is almost as accurate as PBE0 in terms of the mean absolute errors (MAE) of the predicted results with respect to experiment. This result can be understood from the practical effects of correcting the unphysical SIE in both methods. DFT+$U$ method removes SIE by recapturing explicitly the on-site Coulomb repulsion, which suppresses the fractional occupations of the localized orbitals caused by SIE.[76] In contrast, hybrid functionals introduce some part of exact exchange to compensate for the approximate treatment of the electron correlation arising from the antisymmetric nature of the wave functions, where SIE originates.[96] In this way, both

DFT+$U$[16,25] and the hybrid functionals approaches[15,97] reproduce the localization behaviors of the magnetic orbitals along with acceptable $J$ values. It is worthwhile to emphasize that the $U$ correction in DFT+$U$ is applied only within the subspace of correlated orbitals, whereas the exact exchange considered in the hybrid functionals has effects in the whole orbital space. The fact that the two approaches lead to comparable results of $J$ indicates that describing the local Coulomb correlations on the magnetic centers plays a major role in evaluating the magnetic interactions.

Since the experimental $J$s are extracted from the measurement of the molecular crystalline samples,[9,31] we also perform DFT+$U$ calculations with the crystal model (Table 4) to evaluate the crystal packing effects. For some complexes such as XAYTIB, BERPAQ, and FAKLOT, the crystal model calculations slightly overestimate the $J$ values (see Figure 5),
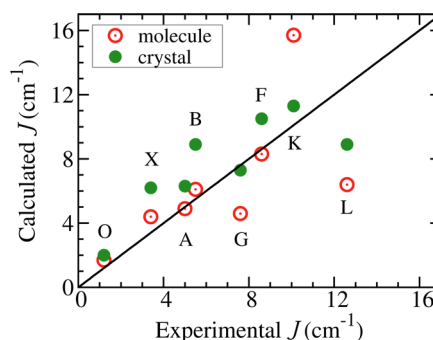


**Figure 5.** Calculated 3d−4f exchange coupling constant $J$ by PBE+$U_{3d4f}$ versus the experimental results. The open (solid) circles refer to results obtained by calculations with the molecular model (crystal model where influence of the crystal packing effects on $J$ can be captured). A single letter is used to denote the ref code of each compound: O (OFELAM), X (XAYTIB), A (AWUQUE), B (BERPAQ), G (GANFIL), F (FAKLOT), K (KEQRED), and L (LAMBUX).

while the molecular model calculations predict better results. For other cases (e.g., GANFIL, KEQRED, and LAMBUX), however, molecular calculations show significant prediction errors, while crystal calculations can provide much improved results. For the whole series of compounds, the crystal model calculations are, in general, slightly more reliable because they decrease the MAE (that is lowered to below 2 cm$^{-1}$) (Table 4), on the one hand, and improve the linear correlation between theory and experiment (Figure 5), on the other hand. The

**Table 4. Calculated 3d−4f Coupling Constants $J^a$ (cm$^{-1}$) Using the Molecular Model (with PBE, PBE+$U^c$, B3LYP, and PBE0) and the Molecular Crystal Model (with PBE+$U$)$^b$**

| ref code | PBE | PBE+$U_{3d}$ | PBE+$U_{4f}$ | PBE+$U_{3d4f}$ | B3LYP | PBE0 | PBE+$U_{3d4f}$ (cryst)$^d$ | expt |
| --- | --- | --- | --- | --- | --- | --- | --- | --- |
| AWUQUE | 3.3 | 3.7 | 4.8 | 4.9 | 1.6 | 3.1 | 6.3 | 5.0 |
| BERPAQ | −2.4 | 5.4 | 0.8 | 6.1 | 3.4 | 4.8 | 8.9 | 5.5 |
| FAKLOT | 7.9 | 7.3 | 10.6 | 8.3 | 6.9 | 7.5 | 10.5 | 8.6 |
| GANFIL | −19.3 | 2.7 | −9.0 | 4.6 | 1.4 | 3.1 | 7.3 | 7.6 |
| KEQRED | 18.8 | 14.5 | 21.2 | 15.7 | 13.1 | 11.5 | 11.3 | 10.1 |
| LAMBUX | 5.4 | 6.1 | 6.9 | 6.4 | 5.5 | 6.5 | 8.9 | 12.6 |
| OFELAM | 0.5 | 1.0 | 1.8 | 1.7 | 1.9 | 2.6 | 2.0 | 1.2 |
| XAYTIB | 1.7 | 4.5 | 2.5 | 4.4 | 9.7 | 7.5 | 6.2 | 3.4 |
| MAE$^e$ | 6.9 | 2.5 | 5.2 | 2.2 | 3.8 | 2.6 | 1.9 | |

$^a$Spin Hamiltonian $\hat{H} = -J\hat{S}_A \cdot \hat{S}_B$. $^b$Experimental values and mean absolute errors (MAE) (cm$^{-1}$) with respect to experiment are also shown. $^c$$U$ is turned on for Cu-3d (PBE+$U_{3d}$), Gd-4f (PBE+$U_{4f}$), and both Cu-3d and Gd-4f (PBE+$U_{3d4f}$). $^d$With molecular crystal model. $^e$Mean absolute error.

**Table 5. Mulliken Charge (Spin) Populations of Gd-4f, Cu-3d, O-2p (Bridge Atom Linking Cu and Gd), and Gd-5d of the Model Compound GANFIL in Both HS and BS[a] States Calculated by PBE and PBE+$U$**

| method | Gd-4f | Cu-3d | O-2p | Gd-5d |
|---|---|---|---|---|
| PBE | | | | |
| HS | 7.043 (6.909)[b] | 9.401 (0.549) | 4.604 (0.094) | 0.808 (0.076) |
| BS | 7.045 (6.907) | 9.405 (−0.539)[c] | 4.604 (−0.098) | 0.808 (0.074) |
| PBE+$U_{3d}$ | | | | |
| HS | 7.045 (6.911) | 9.310 (0.716) | 4.624 (0.060) | 0.810 (0.078) |
| BS | 7.046 (6.910) | 9.313 (−0.713) | 4.625 (−0.065) | 0.806 (0.070) |
| PBE+$U_{4f}$ | | | | |
| HS | 7.017 (6.955) | 9.401 (0.549) | 4.606 (0.092) | 0.819 (0.073) |
| BS | 7.019 (6.953) | 9.400 (−0.540) | 4.606 (−0.102) | 0.819 (0.069) |
| PBE+$U_{3d4f}$ | | | | |
| HS | 7.018 (6.952) | 9.310 (0.716) | 4.626 (0.060) | 0.817 (0.073) |
| BS | 7.019 (6.953) | 9.311 (−0.715) | 4.627 (−0.065) | 0.821 (0.069) |

[a]Obtained by flipping the spin moment on Cu center. [b]Spin populations presented in parentheses. [c]Negative values indicate down-spin populations.
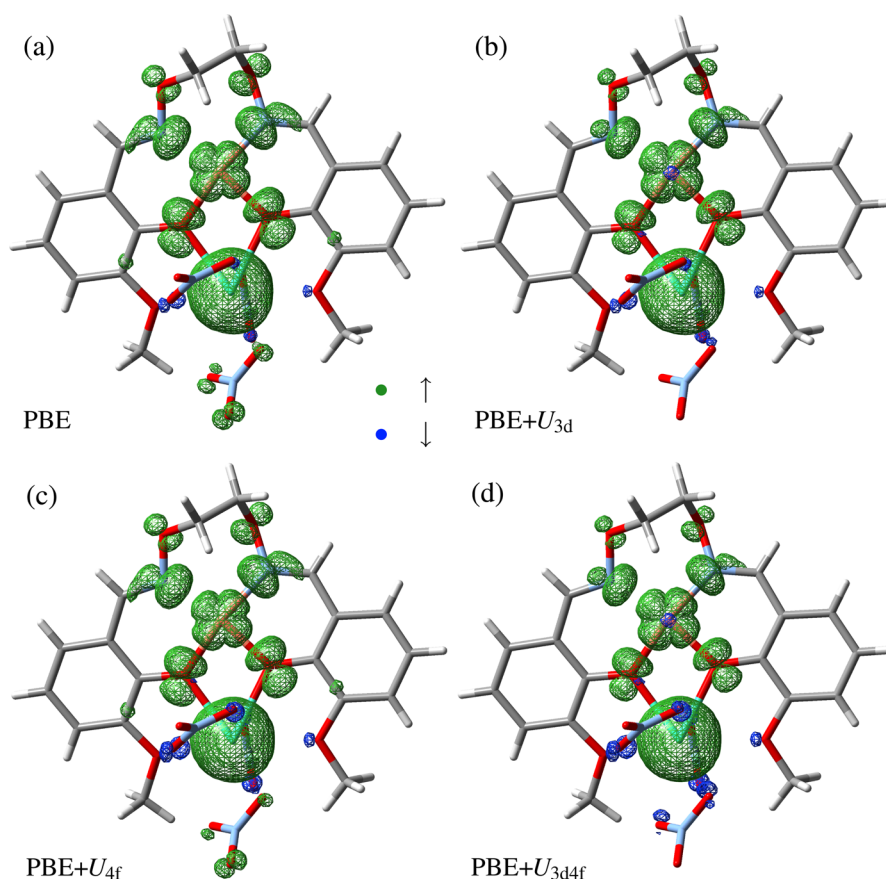


**Figure 6.** Spin densities of the model molecule GANFIL in the HS state (those in the BS state are provided in the Supporting Information) calculated by PBE (a), PBE+$U_{3d}$ (b), PBE+$U_{4f}$ (c), and PBE+U$_{3d4f}$ (d). The isosurface represents a magnitude of 0.002 $e$/bohr$^3$. ↑ and ↓ denote up-spin and down-spin densities, respectively.

better agreement between theory and experiment achieved in our study should be attributed to the fact that the crystal model is closer to the real system.

The influence of the crystal packing effects on $J$ results essentially from the Coulomb interaction nature of the exchange coupling and its close relationship with the chemical bonds.[98] Compared to the isolated molecular case, both the ligand fields around the magnetic centers and the electron densities on the chemical links bridging the interacting spin carriers will be slightly modified by the secondary coordination environments (e.g., H-bonding network) in crystalline materials. It has been identified that the H-bonding can effectively tune the magnetic coupling[99] or even mediate the exchange interactions between magnetic centers in different molecules.[100] Thus, the exchange interactions mediated by the metal−ligand bonds should be more or less different from those in the isolated molecular entities depending on the degree of the electron redistributions upon packing the molecules.

**3.3. Physical Effects of $U$.** In the following, we take the compound GANFIL as a model system to analyze the physical effects of $U$ and to explore the 3d−4f exchange pathways in the
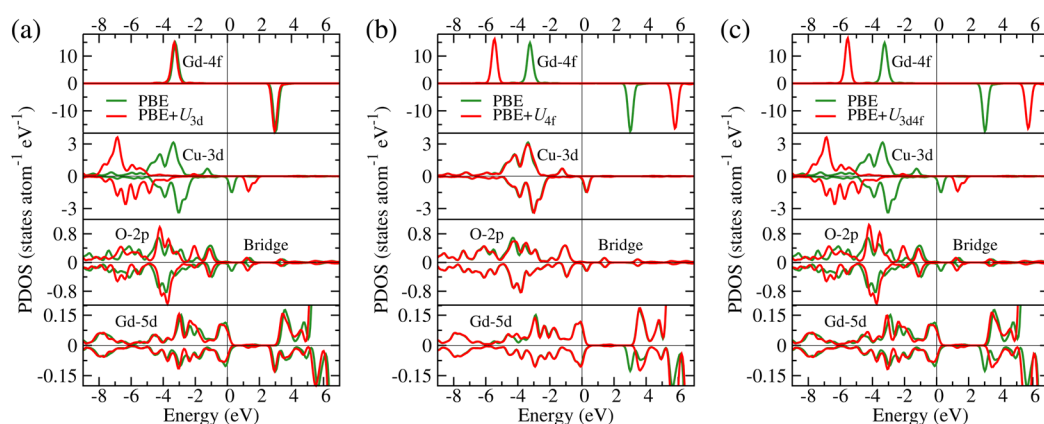
**Figure 7.** Comparison of the projected density of states (PDOS) of GANFIL in the HS state (those in the BS state are provided in the Supporting Information) calculated by PBE and PBE+$U$ ((a) PBE+$U_{3d}$, (b) PBE+$U_{4f}$, and (c) PBE+$U_{3d4f}$). From top to bottom panels, Gd-4f, Cu-3d, bridge O-2p, and Gd-5d orbitals are shown. The energy scales are shifted with respect to the valence band maxima (VBM) that are set to 0 eV. Positive and negative values denote majority- and minority-spin states. The intersections between the VBM line and the expanded 5d bands result from the artificial (Gaussian) broadening (by 0.2 eV) of the eigenvalues to get smooth PDOS.

Cu(II)−Gd(III) compounds. We concentrate on the changes of charge/spin populations (Mulliken populations (Table 5)), spin densities (Figure 6), and electronic structures (projected density of states (PDOS) in Figure 7). The Hubbard $U$ corrections are imposed selectively on Cu-3d, Gd-4f, or both of them, which are denoted by $U_{3d}$, $U_{4f}$, and $U_{3d4f}$, respectively.

First, both 4f- and 3d-spin magnetic moments are increased by $U$. That is because $U$ shifts the occupied 3d/4f states to lower energies while shifting the unoccupied 3d/4f states toward higher energies (Figure 7). In the HS state, for example, the unoccupied states for both the 4f and the 3d orbitals belong to the minority-spin states, whose populations are decreased by 0.036 and 0.129 for 4f and 3d, respectively, after $U$ is imposed. Meanwhile, the majority-spin populations are increased by 0.010 and 0.038 for 4f and 3d. The population decrease of the minority-spin states is larger than the population increase of the majority-spin states. Therefore, we can see decreased charge populations while increased spin populations on both the Gd-4f and the Cu-3d orbitals when $U$ is turned on locally (Table 5). However, the influence of $U_{4f}$ on populations of 3d is negligible and so is $U_{3d}$ on the populations of the 4f orbitals. It proves that direct interactions between 3d and 4f are insignificant for the 3d−4f exchange coupling.[28]

Second, the charge/spin populations on the bridge O-2p orbitals are significantly changed by $U_{3d}$. In particular, $U_{3d}$ largely reduces the spin density on the bridge O-2p orbitals because it suppresses the spin delocalization effect of the 3d orbitals. When we flip the spin moment on the Cu-3d orbitals in the BS state, the spin moment on O-2p is also flipped correspondingly (Table 5). Thus, the spin distributions on the bridge O atoms are dominated by Cu-3d (see the spin densities for the whole molecule obtained with PBE (Figure 6a), PBE +$U_{3d}$ (Figure 6b), PBE+$U_{4f}$ (Figure 6c), and PBE+$U_{3d4f}$ (Figure 6d)).

In contrast, $U_{4f}$ slightly decreases the spin up density on O-2p in the HS state or increases the spin down density in the BS state, which is shown by comparing the PBE+$U_{4f}$ with the PBE results (Table 5). This phenomenon probably results from the spin polarization effect[30,101] induced by the 4f orbitals, which always leads to antiparallel spin magnetic moments on the surrounding ligands with respect to the Ln center. The spin polarization effect originates from the hybridization between

the ligand orbitals and the expanded Ln-5d orbitals. The majority-spin electrons transferred from the ligands to the empty 5d orbitals are stabilized by the like-spin 4f electrons due to the intra-atomic exchange coupling according to the Hund's rule, so that the minority-spin electrons are slightly dominant on the ligands. We find that this effect tends to be enhanced by $U_{4f}$ (Figure 6a vs Figure 6c and Figure 6b vs Figure 6d). The reason is that by switching on $U_{4f}$, 4f orbitals become more atomic-like, resulting in the strengthened 4f−5d ferromagnetic exchange coupling,[102] which in turn promotes the spin polarization. Besides, the charge population on 5d is modified to a larger extent by $U_{4f}$ than by $U_{3d}$, showing that 4f−5d coupling, as stressed in ref 13, contributes more to the 5d occupations than the 3d−5d charge transfer.[19]

From the electronic structures point of view, the Hubbard $U$ lowers the occupied energy levels of both 4f and 3d while shifting their unoccupied orbitals toward higher energies with respect to the valence band maxima (comparison of the PDOS from PBE and PBE+$U$ ($U_{3d}$, $U_{4f}$, and $U_{3d4f}$) presented in Figure 7a,b,c, respectively), and therefore weakens their hybridization with the outer valence or ligand orbitals. The O-2p bands are narrowed considerably by $U_{3d}$ (Figure 7a), which shows that 3d and 2p orbitals form chemical bonds directly. Correspondingly, there are observable variation in the occupied 5d bands, indicating direct 5d−2p hybridization. In contrast, both the 2p and the 5d bands respond rather weakly to $U_{4f}$ (Figure 7b). It indicates that direct 4f−2p interactions are negligible and that the 4f−5d overlap is also not effective.

Next, we relate the above findings to the variation of $J$ caused by $U$. For GANFIL, both $U_{3d}$ and $U_{4f}$ increase $J$. For the whole series of the model compounds, $U_{3d}$ either increases or decreases the $J$ values, while $U_{4f}$ almost consistently increases them (Table 4). On the basis of these effects, we can identify two competing magnetic exchange pathways, denoted as A and B (Figure 8). In pathway A, the minority-spin O-2p orbital hybridizes with the like-spin Cu-3d orbital; the majority-spin O-2p orbital interacts with the like-spin Gd-5d orbital whose spin moment couples ferromagnetically with the Gd-4f spin moment. This pathway is effective when the magnetic moments on Cu and Gd are parallel and thus results in ferromagnetic (FM) contribution. In pathway B, the majority-spin O-2p orbital hybridizes with the like-spin Cu-3d orbital, while the
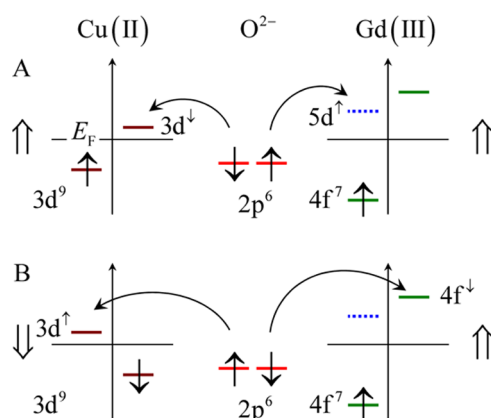
**Figure 8.** Two exchange pathways of the 3d−4f magnetic interactions in the Cu(II)−Gd(III) compounds. We employ double up arrow (double down arrow) and ↑ (↓) to denote the spin direction of the magnetic centers and that of the magnetic orbitals, respectively. The vertical axis refers to the energy, and the horizontal line indicates the position of Fermi energy ($E_F$). Orbitals shown below (above) the horizontal line are occupied (unoccupied), and those in the left (right) side are the majority-spin (minority-spin) states. Curved arrows indicate charge transfers from the bridge O atoms to unoccupied orbitals on the magnetic centers. Pathway A is ferromagnetic, while pathway B is antiferromagnetic.

minority-spin O-2p orbital interacts with the empty like-spin Gd-4f orbital. Pathway B only exists in magnetic configurations with antiparallel alignment of the Cu and Gd magnetic moments and leads to antiferromagnetic (AFM) contribution. It has been found that participation of the empty Gd-5d orbitals plays an important role in the FM interactions[19,20,103] and that the overlap of the magnetic orbitals involving 4f contributes to AFM interactions.[30] These findings are well consistent with our proposed exchange pathways.

We recall that $U_{3d}$ largely prevents the spin delocalization effect of the 3d orbitals, so that both pathways are suppressed. Therefore, $J$ can be either increased or decreased by $U_{3d}$ depending on which exchange pathway is suppressed to a larger extent. For most of our model systems under study, $J$ is increased by $U_{3d}$. In rare cases (e.g., the KEQRED molecule), where both Cu···Gd distance and Cu−O−O−Gd dihedral angle are large (Table 1) enough to prevent overlap between magnetic orbitals,[30] pathway B is rather weak and is less affected by $U_{3d}$ than pathway A, such that $J$ is decreased. In contrast, $U_{4f}$, on the one hand, enhances the 4f−5d coupling and thus promotes pathway A, and on the other hand, it shifts the virtual 4f orbitals to higher energy levels, thus suppressing pathway B. Consequently, $J$ is always increased by $U_{4f}$.

Analyzing these two exchange pathways may enable us to better understand the 3d−4f magnetic interactions in the Cu(II)−Gd(III) compounds. On the one hand, participation of the empty 5d orbitals in the Gd−O chemical bonds always contributes to FM interactions. This exchange channel is driven by the intra-atomic 4f−5d FM coupling, and thus the 3d−4f FM exchange part is indirect and weak. On the other hand, because of the planar Cu−O−O−Gd geometry of the Cu−Gd coordination core and the strong localization behavior of the 4f orbitals, overlap of the magnetic orbitals involving 4f is largely prohibited,[20,30] such that the AFM contributions are rather small. As a result, the overall 3d−4f exchange interactions are weak and FM.

Techniques used for investigating the 3d−4f exchange mechanism in previous works involve monitoring the variation of the electron/spin distributions of the systems under study upon some perturbations, such as changing the active orbitals in the CASSCF/CASPT2 calculations[20] or removing the basis sets of specified atomic orbitals.[13] In this work, we employ the Hubbard $U$ as a probe to explore the influence of the local Coulomb correlation on the electronic and magnetic properties of the system, in order to find out the electronic origins of the exchange interactions. Our approach represents an alternative way to study the mechanism of the 3d−4f exchange couplings. The advantages of this approach include the following: (i) the DFT+$U$ calculations are very efficient; (ii) the Hubbard $U$ is physically transparent; and (iii) it can be readily extended to more complicated systems.

## 4. CONCLUSIONS

In summary, the 3d−4f exchange interactions in a series of Cu(II)−Gd(III) compounds are studied using the DFT+$U$ approach based on the PAO-NCPP method. We close this article with the following conclusions. First, inclusion of the 5s5p shells in the valence region of the Gd-pseudopotential is necessary for an accurate description of the 4f orbitals. Second, PBE+$U$ calculations can reproduce the experimental 3d−4f interactions as accurately as the hybrid functionals B3LYP and PBE0, indicating the importance of the accurate description of the local Coulomb correlations within the magnetic centers in evaluating $J$. Third, solid state calculations using the crystal model predict overall better results than those with the molecular model, showing the influence of the crystal packing effects on $J$. Finally, by analyzing the effects of $U$, we identify two competing magnetic exchange pathways. One involves an interaction between the Cu-3d, O-2p, and the empty Gd-5d orbitals and leads to a ferromagnetic contribution. The other one involves the Cu-3d, O-2p, and the empty Gd-4f orbitals and is antiferromagnetic. These findings are useful for a better understanding of the mechanism of the ferromagnetic 3d−4f exchange interactions. This study shows the DFT+$U$ method to be very promising for investigating the exchange interactions in the 3d−4f molecular materials.

## ■ ASSOCIATED CONTENT

**⑤ Supporting Information**

Computational setup details about the test calculations of the Gd-PPs, spin density, and PDOS of the model compound GANFIL in the BS state, xyz files of all model compounds investigated in this work, and sample inputs for the calculations of $J$ in both SIESTA and ORCA. This material is available free of charge via the Internet at http://pubs.acs.org.

## ■ AUTHOR INFORMATION

**Corresponding Author**

*(H.J.) E-mail: h.jiang@pku.edu.cn.

**Present Address**

†Duke University, Durham, North Carolina 27708, United States.

**Notes**

The authors declare no competing financial interest.

## ■ ACKNOWLEDGMENTS

# ■ REFERENCES

(1) Peng, J.-B.; Zhang, Q.-C.; Kong, X.-J.; Zheng, Y.-Z.; Ren, Y.-P.; Long, L.-S.; Huang, R.-B.; Zheng, L.-S.; Zheng, Z. High-Nuclearity 3d−4f Clusters as Enhanced Magnetic Coolers and Molecular Magnets. *J. Am. Chem. Soc.* **2012**, *134*, 3314−3317.

(2) Liu, J.-L.; Lin, W.-Q.; Chen, Y.-C.; Leng, J.-D.; Guo, F.-S.; Tong, M.-L. Symmetry-Related $[Ln_6^{III} Mn_{12}^{III}]$ Clusters toward Single-Molecule Magnets and Cryogenic Magnetic Refrigerants. *Inorg. Chem.* **2013**, *52*, 457−463.

(3) Andruh, M.; Costes, J. P.; Diaz, C.; Gao, S. 3d−4f Combined Chemistry: Synthetic Strategies and Magnetic Properties. *Inorg. Chem.* **2009**, *48*, 3342−3359.

(4) Liu, Y.; Chen, Z.; Ren, J.; Zhao, X.-Q.; Cheng, P.; Zhao, B. Two-Dimensional 3d−4f Networks Containing Planar $Co_4Ln_2$ Clusters with Single-Molecule-Magnet Behaviors. *Inorg. Chem.* **2012**, *51*, 7433−7435.

(5) Feltham, H. L. C.; Clérac, R.; Ungur, L.; Chibotaru, L. F.; Powell, A. K.; Brooker, S. By Design: A Macrocyclic 3d−4f Single-Molecule Magnet with Quantifiable Zero-Field Slow Relaxation of Magnetization. *Inorg. Chem.* **2013**, *52*, 3236−3240.

(6) Sessoli, R.; Powell, A. K. Strategies towards Single Molecule Magnets Based on Lanthanide Ions. *Coord. Chem. Rev.* **2009**, *253*, 2328−2341.

(7) Zheng, Y.-Z.; Evangelisti, M.; Winpenny, R. E. P. Co−Gd Phosphonate Complexes as Magnetic Refrigerants. *Chem. Sci.* **2011**, *2*, 99−102.

(8) Langley, S. K.; Chilton, N. F.; Moubaraki, B.; Hooper, T.; Brechin, E. K.; Evangelisti, M.; Murray, K. S. Molecular Coolers: The Case for $[Cu_5^{II} Gd_4^{III}]$. *Chem. Sci.* **2011**, *2*, 1166−1169.

(9) Sutter, J.-P.; Kahn, M. L. In *Magnetism: Molecules to Materials V*; Miller, J. S., Drillon, M., Eds.; Wiley-VCH: Weinheim, Germany, 2005; Chapter 5, pp 161−187.

(10) Ruiz, E.; Alvarez, S.; Rodríguez-Fortea, A.; Alemany, P.; Pouillon, Y.; Massobrio, C. In *Magnetism: Molecules to Materials II*; Miller, J. S., Drillon, M., Eds.; Wiley-VCH: Weinheim, Germany, 2001; Chapter 7, pp 227−279.

(11) Ruiz, E.; Rodríguez-Fortea, A.; Cano, J.; Alvarez, S.; Alemany, P. About the Calculation of Exchange Coupling Constants in Polynuclear Transition Metal Complexes. *J. Comput. Chem.* **2003**, *24*, 982−989.

(12) Sessoli, R. Chilling with Magnetic Molecules. *Angew. Chem., Int. Ed.* **2012**, *51*, 43−45.

(13) Cremades, E.; Gómez-Coca, S.; Aravena, D.; Alvarez, S.; Ruiz, E. Theoretical Study of Exchange Coupling in 3d-Gd Complexes: Large Magnetocaloric Effect Systems. *J. Am. Chem. Soc.* **2012**, *134*, 10532−10542.

(14) Richter, M. Band Structure Theory of Magnetism in 3d−4f Compounds. *J. Phys. D: Appl. Phys.* **1998**, *31*, 1017.

(15) Martin, R. L.; Illas, F. Antiferromagnetic Exchange Interactions from Hybrid Density Functional Theory. *Phys. Rev. Lett.* **1997**, *79*, 1539−1542.

(16) Postnikov, A. V.; Bihlmayer, G.; Blügel, S. Exchange Parameters in Fe-Based Molecular Magnets. *Comput. Mater. Sci.* **2006**, *36*, 91−95.

(17) Perdew, J. P.; Zunger, A. Self-Interaction Correction to Density-Functional Approximations for Many-Electron Systems. *Phys. Rev. B* **1981**, *23*, 5048−5079.

(18) Cohen, A. J.; Mori-Sánchez, P.; Yang, W. Insights into Current Limitations of Density Functional Theory. *Science* **2008**, *321*, 792−794.

(19) Rajaraman, G.; Totti, F.; Bencini, A.; Caneschi, A.; Sessoli, R.; Gatteschi, D. Density Functional Studies on the Exchange Interaction of a Dinuclear Gd(III)−Cu(II) Complex: Method Assessment, Magnetic Coupling Mechanism and Magneto-Structural Correlations. *Dalton Trans.* **2009**, 3153−3161.

(20) Paulovič, J.; Cimpoesu, F.; Ferbinteanu, M.; Hirao, K. Mechanism of Ferromagnetic Coupling in Copper(II)−Gadolinium-(III) Complexes. *J. Am. Chem. Soc.* **2004**, *126*, 3321−3331.

(21) Lüders, M.; Ernst, A.; Däne, M.; Szotek, Z.; Svane, A.; Ködderitzsch, D.; Hergert, W.; Györffy, B. L.; Temmerman, W. M. Self-Interaction Correction in Multiple Scattering Theory. *Phys. Rev. B* **2005**, *71*, 205109.

(22) Hughes, I. D.; Däne, M.; Ernst, A.; Hergert, W.; Lüders, M.; Poulter, J.; Staunton, J. B.; Svane, A.; Szotek, Z.; Temmerman, W. M. Lanthanide Contraction and Magnetism in the Heavy Rare Earth Elements. *Nature* **2007**, *446*, 650−653.

(23) Anisimov, V. I.; Aryasetiawan, F.; Lichtenstein, A. I. First-Principles Calculations of the Electronic Structure and Spectra of Strongly Correlated Systems: The LDA+U Method. *J. Phys.: Condens. Matter* **1997**, *9*, 767.

(24) Larson, P.; Lambrecht, W. R. L.; Chantis, A.; van Schilfgaarde, M. Electronic Structure of Rare-Earth Nitrides Using the LSDA+U Approach: Importance of Allowing 4f Orbitals to Break the Cubic Crystal Symmetry. *Phys. Rev. B* **2007**, *75*, 045114.

(25) Zhang, Y.; Jiang, H. Intra- and Interatomic Spin Interactions by the Density Functional Theory Plus U Approach: A Critical Assessment. *J. Chem. Theory Comput.* **2011**, *7*, 2795−2803.

(26) Jeschke, H. O.; Salvat-Pujol, F.; Valentí, R. First-Principles Determination of Heisenberg Hamiltonian Parameters for the Spin-1/2 Kagome Antiferromagnet $ZnCu_3(OH)_6Cl_2$. *Phys. Rev. B* **2013**, *88*, 075106.

(27) Reiher, M.; Wolf, A. *Relativistic Quantum Chemistry: The Fundamental Theory of Molecular Science*; Wiley-VCH: Weinheim, Germany, 2009.

(28) Benelli, C.; Gatteschi, D. Magnetism of Lanthanides in Molecular Materials with Transition-Metal Ions and Organic Radicals. *Chem. Rev.* **2002**, *102*, 2369−2388.

(29) Van Vleck, J. H. *The Theory of Electric and Magnetic Susceptibilities*; Oxford University Press: Oxford, U.K., 1965.

(30) Cirera, J.; Ruiz, E. Exchange Coupling in $Cu^{II}Gd^{III}$ Dinuclear Complexes: A Theoretical Perspective. *C. R. Chim.* **2008**, *11*, 1227−1234.

(31) Kahn, O. *Molecular Magnetism*; VCH Publishers, Inc.: New York, 1993.

(32) van Lenthe, E.; Baerends, E. J.; Snijders, J. G. Relativistic Regular Two-Component Hamiltonians. *J. Chem. Phys.* **1993**, *99*, 4597.

(33) Douglas, M.; Kroll, N. M. Quantum Electrodynamical Corrections to the Fine Structure of Helium. *Ann. Phys.* **1974**, *82*, 89−155.

(34) Hess, B. A. Relativistic Electronic-Structure Calculations Employing a Two-Component No-Pair Formalism with External-Field Projection Operators. *Phys. Rev. A* **1986**, *33*, 3742.

(35) Hay, P. J.; Wadt, W. R. Ab Initio Effective Core Potentials for Molecular Calculations. Potentials for the Transition Metal Atoms Sc To Hg. *J. Chem. Phys.* **1985**, *82*, 270.

(36) Fuentealba, P.; Preuss, H.; Stoll, H.; Von Szentpály, L. A Proper Account of Core- Polarization with Pseudopotentials: Single Valence-Electron Alkali Compounds. *Chem. Phys. Lett.* **1982**, *89*, 418−422.

(37) Singh, D. J.; Nordström, L. Planewaves. *Pseudopotentials, and the LAPW method*, 2nd ed.; Springer: New York, 2006.

(38) Martin, R. M. *Electronic Structure: Basic Theory and Practical Methods*; Cambridge University Press: Cambridge, U.K., 2004; Chapter 11, pp 204−231.

(39) Meyer, B. In *Computational Nanoscience: Do It Yourself!*; Grotendorst, J., Blügel, S., Marx, D., Eds.; NIC Series, 2006; Vol. 31, pp 71−83.

(40) Pollet, R.; Clavaguéra, C.; Dognon, J. P. Ultrasoft Pseudopotentials for Lanthanide Solvation Complexes: Core or Valence Character of the 4f Electrons. *J. Chem. Phys.* **2006**, *124*, 164103.

(41) Pollet, R.; Marx, D. Ab Initio Simulation of a Gadolinium-Based Magnetic Resonance Imaging Contrast Agent in Aqueous Solution. *J. Chem. Phys.* **2007**, *126*, 181102.

(42) Cundari, T. R.; Stevens, W. J. Effective Core Potential Methods for the Lanthanides. *J. Chem. Phys.* **1993**, *98*, 5555.

(43) Xu, W.; Ji, W.-X.; Qiu, Y.-X.; Schwarz, W. E.; Wang, S.-G. On Structure and Bonding of Lanthanoid Trifluorides $LnF_3$ (Ln = La to Lu). *Phys. Chem. Chem. Phys.* **2013**, *15*, 7839−7847.

(44) Pickard, C. J.; Winkler, B.; Chen, R. K.; Payne, M. C.; Lee, M. H.; Lin, J. S.; White, J. A.; Milman, V.; Vanderbilt, D. Structural Properties of Lanthanide and Actinide Compounds within the Plane Wave Pseudopotential Approach. *Phys. Rev. Lett.* **2000**, *85*, 5122−5125.

(45) Loison, C.; Leithe-Jasper, A.; Rosner, H. Electronic Structures of Intermetallic Borides $RPd_3B_x$ (R = Rare-Earth Metals). *Phys. Rev. B* **2007**, *75*, 205135.

(46) Hamann, D. R.; Schlüter, M.; Chiang, C. Norm-Conserving Pseudopotentials. *Phys. Rev. Lett.* **1979**, *43*, 1494−1497.

(47) Soler, J. M.; Artacho, E.; Gale, J. D.; García, A.; Junquera, J.; Ordejón, P.; Sánchez- Portal, D. The SIESTA Method for ab Initio Order-N Materials Simulation. *J. Phys.: Condens. Matter* **2002**, *14*, 2745.

(48) Troullier, N.; Martins, J. L. Efficient Pseudopotentials for Plane-Wave Calculations. *Phys. Rev. B* **1991**, *43*, 1993−2006.

(49) Louie, S. G.; Froyen, S.; Cohen, M. L. Nonlinear Ionic Pseudopotentials in Spin-Density-Functional Calculations. *Phys. Rev. B* **1982**, *26*, 1738−1742.

(50) Blöchl, P. E. Projector Augmented-Wave Method. *Phys. Rev. B* **1994**, *50*, 17953.

(51) Kresse, G.; Joubert, D. From Ultrasoft Pseudopotentials to the Projector Augmented-Wave Method. *Phys. Rev. B* **1999**, *59*, 1758.

(52) Kresse, G.; Furthmüller, J. Efficiency of ab-Initio Total Energy Calculations for Metals and Semiconductors Using a Plane-Wave Basis Set. *Comput. Mater. Sci.* **1996**, *6*, 15−50.

(53) Kresse, G.; Furthmüller, J. Efficient Iterative Schemes for ab Initio Total-Energy Calculations Using a Plane-Wave Basis Set. *Phys. Rev. B* **1996**, *54*, 11169−11186.

(54) Hafner, J. Materials Simulations Using VASP−A Quantum Perspective to Materials Science. *Comput. Phys. Commun.* **2007**, *177*, 6−13.

(55) Pseudopotential and Basis Set Databases Home Page. http://departments.icmab.es/leem/siesta/Databases/index.html (accessed July 1, 2010).

(56) Costes, J.-P.; Dahan, F.; Novitchi, G.; Arion, V.; Shova, S.; Lipkowski, J. Macrocyclic and Open-Chain $Cu^{II}$-4f (4f = $Gd^{III}$, $Ce^{III}$) Complexes with Planar Diamino Chains: Structures and Magnetic Properties. *Eur. J. Inorg. Chem.* **2004**, *2004*, 1530−1537.

(57) Novitchi, G.; Costes, J.-P.; Donnadieu, B. Synthesis and Structure of 1-D Heterometallic Thiocyanato-Bridged $Cu^{II}Gd^{III}$ Polymers with Ferromagnetic Properties. *Eur. J. Inorg. Chem.* **2004**, *2004*, 1808−1812.

(58) Costes, J.-P.; Novitchi, G.; Shova, S.; Dahan, F.; Donnadieu, B.; Tuchagues, J.-P. Synthesis, Structure, and Magnetic Properties of Heterometallic Dicyanamide-Bridged Cu−Na and Cu−Gd One-Dimensional Polymers. *Inorg. Chem.* **2004**, *43*, 7792−7799.

(59) Akine, S.; Matsumoto, T.; Taniguchi, T.; Nabeshima, T. Synthesis, Structures, and Magnetic Properties of Tri- and Dinuclear Copper(II)−Gadolinium(III) Complexes of Linear Oligooxime Ligands. *Inorg. Chem.* **2005**, *44*, 3270−3274.

(60) Costes, J.-P.; Dahan, F.; Dupuis, A. Influence of Anionic Ligands (X) on the Nature and Magnetic Properties of Dinuclear $LCuGdX_3$·$nH_2O$ Complexes ($LH_2$ Standing for Tetradentate Schiff Base Ligands Deriving from 2-Hydroxy-3-methoxybenzaldehyde and X Being Cl, $N_3C_2$, and $CF_3COO$). *Inorg. Chem.* **2000**, *39*, 165−168.

(61) Koner, R.; Lee, G.-H.; Wang, Y.; Wei, H.-H.; Mohanta, S. Two New Diphenoxo-Bridged Discrete Dinuclear $Cu^{II}Gd^{III}$ Compounds with Cyclic Diimino Moieties: Syntheses, Structures, and Magnetic Properties. *Eur. J. Inorg. Chem.* **2005**, *2005*, 1500−1505.

(62) Ryazanov, M.; Nikiforov, V.; Lloret, F.; Julve, M.; Kuzmina, N.; Gleizes, A. Magnetically Isolated $Cu^{II}Gd^{III}$ Pairs in the Series [Cu(acacen)Gd(pta)$_3$], [Cu(acacen)Gd(hfa)$_3$], [Cu(salen)Gd(pta)$_3$], and [Cu(salen)Gd(hfa)$_3$], [acacen = $N,N'$- Ethylenebis-(acetylacetoniminate(−)), salen = $N,N'$-Ethylenebis-(salicylideniminate(−)), hfa = 1,1,1,5,5,5-Hexafluoropentane-2,4-dio-nate(−), pta = 1,1,1-Trifluoro-5,5-dimethylhexane- 2,4-dionate(−)]. *Inorg. Chem.* **2002**, *41*, 1816−1823.

(63) He, F.; Tong, M.-L.; Chen, X.-M. Synthesis, Structures, and Magnetic Properties of Heteronuclear Cu(II)−Ln(III) (Ln = La, Gd, or Tb) Complexes. *Inorg. Chem.* **2005**, *44*, 8285−8292.

(64) Noodleman, L. Valence Bond Description of Antiferromagnetic Coupling in Transition Metal Dimers. *J. Chem. Phys.* **1981**, *74*, 5737.

(65) Ruiz, E.; Cano, J.; Alvarez, S.; Alemany, P. Broken Symmetry Approach to Calculation of Exchange Coupling Constants for Homobinuclear and Heterobinuclear Transition Metal Complexes. *J. Comput. Chem.* **1999**, *20*, 1391−1400.

(66) Perdew, J. P.; Burke, K.; Ernzerhof, M. Generalized Gradient Approximation Made Simple. *Phys. Rev. Lett.* **1996**, *77*, 3865−3868.

(67) Artacho, E.; Gale, J. D.; García, A.; Junquera, J.; Martin, R. M.; Ordejón, P.; Sánchez- Portal, D.; Soler, J. M. Siesta Downloads Home Page. http://departments.icmab.es/leem/siesta/CodeAccess/Code/downloads.html (accessed August 1, 2010).

(68) Junquera, J.; Paz, O.; Sánchez-Portal, D.; Artacho, E. Numerical Atomic Orbitals for Linear-Scaling Calculations. *Phys. Rev. B* **2001**, *64*, 235111.

(69) This parameter refers to the energy increase of the eigenvalues of the basis orbitals due to the effects of the confinement. The smaller this value is, the more similar the pseudoatomic obritals become to the real atomic orbitals.

(70) Artacho, E.; Sánchez-Portal, D.; Ordejón, P.; García, A.; Soler, J. M. Linear-Scaling ab Initio Calculations for Large and Complex Systems. *Phys. Status Solidi B* **1999**, *215*, 809−817.

(71) This parameter is provided as an energy cutoff, which is equal to the maximum energy of the plane waves represented in the defined grid spacing. A higher value provides finer grid and better accuracy but requires more computational efforts.

(72) Dudarev, S. L.; Botton, G. A.; Savrasov, S. Y.; Humphreys, C. J.; Sutton, A. P. Electron-Energy-Loss Spectra and the Structural Stability of Nickel Oxide: An LSDA+U Study. *Phys. Rev. B* **1998**, *57*, 1505−1509.

(73) Anisimov, V. I.; Zaanen, J.; Andersen, O. K. Band Theory and Mott Insulators: Hubbard U Instead of Stoner I. *Phys. Rev. B* **1991**, *44*, 943−954.

(74) Liechtenstein, A. I.; Anisimov, V. I.; Zaanen, J. Density-Functional Theory and Strong Interactions: Orbital Ordering in Mott−Hubbard Insulators. *Phys. Rev. B* **1995**, *52*, R5467−R5470.

(75) Tablero, C. Representations of the Occupation Number Matrix on the LDA/GGA+U Method. *J. Phys.: Condens. Matter* **2008**, *20*, 325205.

(76) Cococcioni, M.; de Gironcoli, S. Linear Response Approach to the Calculation of the Effective Interaction Parameters in the LDA+U Method. *Phys. Rev. B* **2005**, *71*, 035105.

(77) Hüfner, S. *Photoelectron Spectroscopy: Principles and Applications*, 3rd ed.; Springer Verlag: Weinheim, Germany, 2003.

(78) Dederichs, P. H.; Blügel, S.; Zeller, R.; Akai, H. Ground States of Constrained Systems: Application to Cerium Impurities. *Phys. Rev. Lett.* **1984**, *53*, 2512−2515.

(79) Anisimov, V. I.; Gunnarsson, O. Density-Functional Calculation of Effective Coulomb Interactions in Metals. *Phys. Rev. B* **1991**, *43*, 7570−7574.

(80) Solovyev, I. V.; Dederichs, P. H.; Anisimov, V. I. Corrected Atomic Limit in the Local- Density Approximation and the Electronic Structure of d Impurities in Rb. *Phys. Rev. B* **1994**, *50*, 16861−16871.

(81) Pickett, W. E.; Erwin, S. C.; Ethridge, E. C. Reformulation of the LDA+U Method for a Local-Orbital Basis. *Phys. Rev. B* **1998**, *58*, 1201−1209.

(82) Aryasetiawan, F.; Imada, M.; Georges, A.; Kotliar, G.; Biermann, S.; Lichtenstein, A. I. Frequency-Dependent Local Interactions and Low-Energy Effective Models from Electronic Structure Calculations. *Phys. Rev. B* **2004**, *70*, 195104.

(83) Karlsson, K.; Aryasetiawan, F.; Jepsen, O. Method for Calculating the Electronic Structure of Correlated Materials from a Truly First-Principles LDA+U Scheme. *Phys. Rev. B* **2010**, *81*, 245113.

(84) Solovyev, I. V.; Dederichs, P. H. Ab Initio Calculations of Coulomb *U* Parameters for Transition-Metal Impurities. *Phys. Rev. B* **1994**, *49*, 6736−6740.

(85) Harmon, B. N.; Antropov, V. P.; Liechtenstein, A. I.; Solovyev, I. V.; Anisimov, V. I. Calculation of Magneto-Optical Properties for 4f Systems: LSDA + Hubbard *U* Results. *J. Phys. Chem. Solids* **1995**, *56*, 1521−1524.

(86) Jiang, H.; Rinke, P.; Scheffler, M. Electronic Properties of Lanthanide Oxides from the *GW* Perspective. *Phys. Rev. B* **2012**, *86*, 125115.

(87) Becke, A. D. Density-Functional Exchange-Energy Approximation with Correct Asymptotic Behavior. *Phys. Rev. A* **1988**, *38*, 3098.

(88) Becke, A. D. Density-Functional Thermochemistry. III. The Role of Exact Exchange. *J. Chem. Phys.* **1993**, *98*, 5648.

(89) Lee, C.; Yang, W.; Parr, R. G. Development of the Colle−Salvetti Correlation-Energy Formula into a Functional of the Electron Density. *Phys. Rev. B* **1988**, *37*, 785.

(90) Adamo, C.; Barone, V. Toward Reliable Density Functional Methods without Adjustable Parameters: The PBE0 Model. *J. Chem. Phys.* **1999**, *110*, 6158.

(91) Adamo, C.; Cossi, M.; Barone, V. An Accurate Density Functional Method for the Study of Magnetic Properties: The PBE0 Model. *J. Mol. Struct.* **1999**, *493*, 145−157.

(92) Neese, F. The ORCA Program System. *Comput. Mol. Sci.* **2012**, *2*, 73−78.

(93) Pantazis, D. A.; Chen, X.-Y.; Landis, C. R.; Neese, F. All-Electron Scalar Relativistic Basis Sets for Third-Row Transition Metal Atoms. *J. Chem. Theory Comput.* **2008**, *4*, 908−919.

(94) Pantazis, D. A.; Neese, F. All-Electron Scalar Relativistic Basis Sets for the Lanthanides. *J. Chem. Theory Comput.* **2009**, *5*, 2229−2238.

(95) Kendall, R. A.; Früchtl, H. A. The Impact of the Resolution of the Identity Approximate Integral Method on Modern ab Initio Algorithm Development. *Theor. Chem. Acc.* **1997**, *97*, 158−163.

(96) Koch, W.; Holthausen, M. C. *A Chemist's Guide to Density Functional Theory*, 2nd ed.; Wiley-VCH: Weinheim, Germany, 2001.

(97) Ruiz, E. Exchange Coupling Constants Using Density Functional Theory: Long-Range Corrected Functionals. *J. Comput. Chem.* **2011**, *32*, 1998−2004.

(98) Goodenough, J. B. *Magnetism and the Chemical Bond*; Interscience Publishers: New York, 1963.

(99) Improta, R.; Kudin, K. N.; Scuseria, G. E.; Barone, V. Structure and Magnetic Properties of Nitroxide Molecular Crystals by Density Functional Calculations Employing Periodic Boundary Conditions. *J. Am. Chem. Soc.* **2002**, *124*, 113−120.

(100) Guennic, B. L.; Amor, N. B.; Maynau, D.; Robert, V. Addressing Through-H Magnetic Interactions: A Comprehensive ab Initio Analysis of This Efficient Coupler. *J. Chem. Theory Comput.* **2009**, *5*, 1506−1510.

(101) Yan, F.; Chen, Z. Magnetic Coupling Constants and Spin Density Maps for Heterobinuclear Complexes GdCu-$(OTf)_3(bdmap)_2(H_2O)\cdot THF$, $[Gd(C_4H_7ON)_4(H_2O)_3]$, $[Fe(CN)_6],2H_2O$, and $[Gd(C_4H_7ON)_4(H_2O)_3][Cr(CN)_6],2H_2O$: A Density Functional Study. *J. Phys. Chem. A* **2000**, *104*, 6295−6300.

(102) In lanthanide atoms, 4f and 5d orbitals are strictly orthogonal, leading to intra-atomic ferromagnetic 4f−5d exchange interaction.

(103) Singh, S. K.; Rajaraman, G. Decisive Interactions that Determine Ferro/Antiferromagnetic Coupling in 3d−4f Pairs: A Case Study on Dinuclear V(IV)−Gd(III) Complexes. *J. Chem. Soc., Dalton Trans.* **2013**, *42*, 3623−3630.